applied sciences

MDPI

Article

Slope Stability Analysis Method of Unsaturated Soil Slopes Considering Pore Gas Pressure Caused by Rainfall Infiltration

Wenjing Tian [1,*], Herman Peiffer [1], Benny Malengier [2], Song Xue [3] and Zhongtian Chen [1]

[1] Department of Civil Engineering, Ghent University, Technologiepark-Zwijnaarde 68, 9052 Ghent, Belgium
[2] Department of Materials, Textiles and Chemical Engineering, Ghent University, Technologiepark-Zwijnaarde 70A, 9052 Ghent, Belgium
[3] Department of Hydraulic & Environment Engineering, China Three Gorges University, Daxuelu Avenue 8, Yichang 443002, China
* Correspondence: wenjing.tian@ugent.be

Abstract: The variation of pore gas pressure caused by rainfall infiltration is an important factor that leads to slope failures. The purpose of this study is to propose a new slope stability analysis method that considers pore gas pressure and examines the effect of airflow on slope stability by using a numerical method. A water-air two-phase flow analysis was conducted to investigate the distribution of pore air pressure, pore water pressure, and water saturation triggered by rainfall infiltration. Then the variation of the load resulting from pore gas pressure was incorporated into the slope stability analysis method based on the unsaturated soil shear strength theory and the residual thrust method to simulate the influence of airflow on the Tanjiahe landslide in China. In order to study the infiltration behavior with respect to initial saturation, water and gas flow analyses were performed considering various initial states of saturation under similar settings. Results showed that the pore gas pressure between the slope surface and the slip band clearly varied and that it decreased during the process from the slide bed to the deep direction. Then, the pore water pressure formed in the saturated zone was transferred by the airflow to the slope toe. As a result, because the pore gas pressure gradient increased the thrust of the slide mass, the safety factor decreased over time. Moreover, in the first step, the magnitude of infiltration decreased with an increase in initial saturation, while when the magnitude dropped to the minimum value, it then went up with an increase in initial saturation. The maximum value was usually reached at a saturation degree of 0% or 100%. When evaluating slope stability, the safety factor obtained by the slope stability analysis method that considered the water-gas coupling effect was much lower than when it was not considered during the process of a similar seepage. The impact on the slope failure was significant and may provide a practical reference for hazard assessments to control rainfall-induced landslides.

Keywords: slope stability; water-gas two-phase flow; residual thrust method; rainfall infiltration; pore gas pressure

check for updates

Citation: Tian, W.; Peiffer, H.; Malengier, B.; Xue, S.; Chen, Z. Slope Stability Analysis Method of Unsaturated Soil Slopes Considering Pore Gas Pressure Caused by Rainfall Infiltration. *Appl. Sci.* **2022**, *12*, 11060. https://doi.org/10.3390/app122111060

Academic Editor: Daniel Dias

Received: 11 October 2022
Accepted: 28 October 2022
Published: 1 November 2022

Publisher's Note: MDPI stays neutral with regard to jurisdictional claims in published maps and institutional affiliations.

Copyright: © 2022 by the authors. Licensee MDPI, Basel, Switzerland. This article is an open access article distributed under the terms and conditions of the Creative Commons Attribution (CC BY) license (https://creativecommons.org/licenses/by/4.0/).

1. Introduction

Slope failures induced by rainfall infiltration are very common all over the world, and the damage raised by such failures can be extremely extensive [1,2]. Based on past research, rainfall infiltration could lead to a high groundwater level, an increase in the unit weight of the sliding soil mass because of the increase in moisture content as well as a decrease in soil shear strength [3,4].

Among all these influences, the rainwater infiltrating the soil and the resulting increment of pore pressure are significant aspects to understand slope failures [5,6]. Two types of pore pressure exist in the soil slope, including pore gas pressure that is present in the unsaturated zone and pore water pressure that is present in the saturated zone. As we all know, soil is a three-phase material that consists of solid particles which make up

the soil skeleton and voids that are filled with air and water. However, when researching infiltration behavior and its impact on slope stability, many scholars choose the one-phase fluid model by analyzing the increase of pore water pressure caused by infiltrated water. In addition, most of them make the assumption that the pore air pressure is equal to atmospheric pressure [7,8]. Recently, there has been a growing interest in the research on the influence of pore gas pressure on slope stability [9]. In order to research the influence of rainfall infiltration on a soil slope, a fully coupled model of water-air two-phase flow should be considered, especially the pore air pressure in the unsaturated zone.

It is difficult to simulate and monitor pore gas pressure in an unsaturated zone. Some studies have been conducted to consider the influence of pore gas pressure as a result of rainfall infiltration acting on soil slopes. Hu et al. [10] proposed a theoretical model to simulate the transfer processes of water and gas in a homogeneous soil slope and to evaluate safety factor variations after long periods of heavy rainfall. Zhang et al. [11] also developed a water-air two-phase flow model to simulate the seepage process and analyzed the variation of pore pressure in the soil. Sun et al. [12] analyzed the characteristics of subsurface airflow triggered by rainfall infiltration and estimated the important effect of airflow on unsaturated soil slope stability. These researchers simulated the infiltration process of water and gas during the infiltration period and verified the important impact of gas pressure.

However, most of these previous studies did not consider pore gas pressure in the slope stability analysis method. There are several methods to evaluate slope stability, including the limit equilibrium condition, the finite element method as well as numerical methods [13]. The limit equilibrium method is considered the most common method adopted by many scholars because of its simplicity and practicability. The residual thrust method is also a commonly used method for a limit equilibrium analysis considering a strip division, which could be suitable for geotechnical slopes where the sliding surface has an arbitrary shape. This method is also recommended by many scholars [14].

In this research, a new slope stability analysis method that considers pore gas pressure was developed and the effect of airflow on slope stability was examined using a numerical analysis. First of all, a water-air two-phase flow analysis was conducted to investigate the distribution of pore air pressure, pore water pressure as well as water saturation induced by rainfall infiltration on unsaturated soil slopes. Then, pore gas pressure was incorporated into the slope stability analysis method on the basis of the unsaturated soil shear strength theory and the residual thrust method for the simulation of the influence of the pore air pressure on the slope stability. After establishing the new method to evaluate the slope stability, a practical engineering slope was adopted to conduct a simulation to research the important impact of pore gas pressure. To understand the infiltration behavior with respect to initial saturation, water flow and airflow analyses and the analysis of the magnitude of infiltration were also performed with different initial saturation under similar settings in this paper.

2. Computational Model

2.1. Differential Equations for the Control of Water and Gas

According to the principle of continuum mechanics [15], soil can be considered as a continuum composed of three independent phases, including solid, liquid, and gas phases. If the soil was saturated, the voids would be completely occupied by water; if the soil was dry, the voids would be full of air and water, or the soil would be partially saturated.

While the flow of the liquid phase is driven by gravity and the water pressure gradient, it could also be affected by the pore characteristics of the soil, moisture conditions, and the viscosity of the water phase. According to the law of conservation of mass, the liquid flow equation could be expressed as follows [16]:

$$\frac{\partial(\varphi S_r)}{\partial t} + \nabla \cdot \left[-\frac{k_{rw} k}{\mu_w} (\nabla p_w + \rho_w g) \right] - \frac{Q_w}{\rho_w} = 0 \quad (1)$$

where φ is the porosity, S_r is the degree of saturation, μ_w is the viscosity coefficient of the water phase (Pa·s), k_{rw} is the relative permeability coefficient of the water phase, k is the intrinsic permeability of soil (m^2), p_w is the pressure of the water phase (Pa), Q_w is the source of the water phase ($kg/m^3 \cdot s$), ρ_w is the density of the water phase (kg/m^3), and g is the gravitational acceleration (9.8 m/s^2).

The movement of gas in soil is driven by the air pressure gradient. It is also affected by the pore characteristics of the soil, moisture condition, and the viscosity of the gas phase. Based on the law of conservation of mass, the gas flow governing the differential equation could be written as follows [17]:

$$\frac{\partial[(1-S_r)\varphi]}{\partial t} + \nabla \cdot \left[-\frac{k_{rg}k}{\mu_g}(\nabla p_g + \rho_g g) \right] - \frac{Q_g}{\rho_g} = 0 \quad (2)$$

where φ is the porosity, S_r is the degree of saturation, μ_g is the viscosity coefficient of the gas phase (Pa·s), k_{rg} is the relative permeability coefficient of the gas phase, k is the intrinsic permeability of soil (m^2), p_g is the pressure of the gas phase (Pa), Q_g is the source of the gas phase ($kg/(m^3 \cdot s)$), ρ_g is the density of the gas phase (kg/m^3), and g is the gravitational acceleration (9.8 m/s^2).

2.2. Constitutive Model and Parameters

There are five unknown parameters in Equations (1) and (2). In order to solve these two equations, three constitutive equations need to be involved in this calculation, including the soil-water characteristic curve and relative permeability coefficients of water and gas.

2.2.1. Soil-Water Characteristic Curve

The soil-water characteristic curve reflects the relationship between water saturation and matric suction (Figure 1b). A large number of scholars choose the van Genuchten numerical model to describe the relationship between water saturation and matric suction because many researchers have proved that this model is applicable to many soil types. In this research, the matric suction in the soil is defined as $p_c \equiv p_g - p_w$ and the van Genuchten model can be written as follows [18]:

$$p_c = -p_0 \left[\left(\frac{S_r - S_{rw}}{1 - S_{rw}} \right)^{-\frac{1}{m}} - 1 \right]^{1-m} \quad (3)$$

where p_c is the matric suction, p_o is the air-entry pressure, S_{rw} is the residual degree of water saturation, and m is a model parameter related to the material.

2.2.2. Relative Permeability Coefficient of Water

The relationship between the relative flow of water and water saturation can be described by the relative permeability coefficient of water (Figure 1a). In this research, the van Genuchten-Mualem model was selected because of its broad applicability [19].

$$k_{rw} = \left(\frac{S_r - S_{rw}}{1 - S_{rw}} \right)^{0.5} * \left\{ 1 - \left[1 - \left(\frac{S_r - S_{rw}}{1 - S_{rw}} \right)^{1/n} \right]^n \right\}^2 \quad (4)$$

where k_{rw} is the relative permeability coefficient of water and n is a model parameter that is related to the material.

2.2.3. Relative Permeability Coefficient of Gas

The relationship between the relative flow of gas and water saturation can be described by the relative permeability coefficient of gas (Figure 1a). In this study, the Brooks-Corey

model was selected because it works satisfactorily in many cases and has been widely utilized for several decades [20]:

$$k_{rg} = (1 - \frac{S_r - S_{rw}}{1 - S_{rw} - S_{rg}})^{0.5} * [1 - (\frac{S_r - S_{rw}}{1 - S_{rw} - S_{rg}})^{1/m}]^2 \quad (5)$$

where k_{rg} is the relative permeability coefficient of gas, S_{rw} is the residual degree of water saturation, and S_{rg} is the residual degree of air saturation.

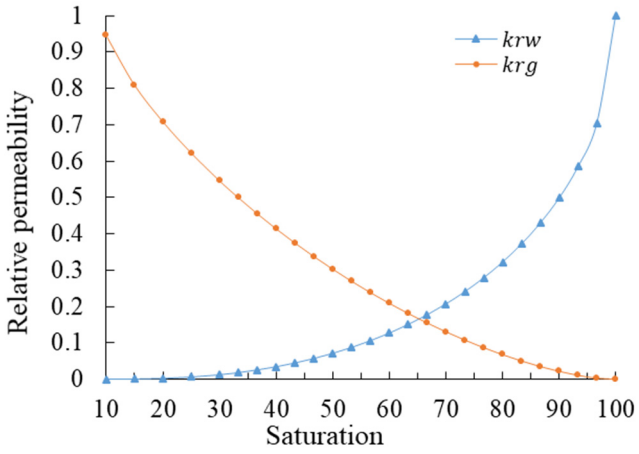

(**a**) Relative permeabilities of water and air

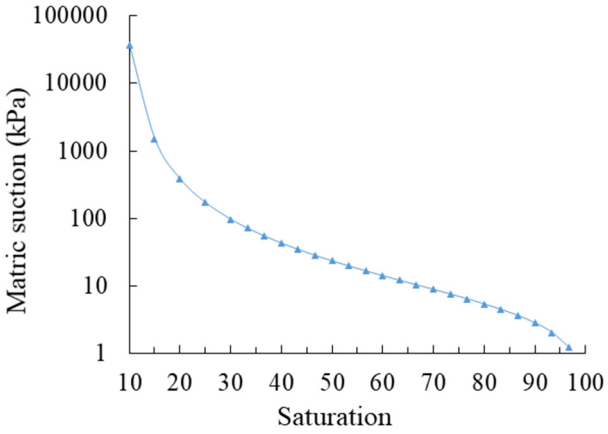

(**b**) Soil-water characteristic curve

Figure 1. Hydraulic characteristics of the seepage analysis.

3. Slope Stability Calculation and Analysis Method

The limit equilibrium method, the finite element method, and numerical methods of modeling are common methods to analyze slope stability. The limit equilibrium method is the most common method that is used by many scholars [21]. According to the principle of strip division, the residual thrust method is also a standard method for a limit equilibrium analysis that is widely used by many scholars.

3.1. Common Slope Stability Analysis Method

In slope stability analysis, the theory of Mohr-Coulomb is used for the distribution of the saturated soil shear strength. In many cases, effective stress is considered the only stress variable, in particular in a detailed analysis. However, the traditional Mohr-Coulomb theory is not utilized in unsaturated soil slope engineering. In order to analyze the contributions of matric suction and pore air pressure to shear strength, the modified Mohr-Coulomb

failure criterion is written as follows, using two independent stress variables, including effective stress and matric suction [22]:

$$\tau = c' + (\sigma - p_a)tan\varphi' + (p_a - p_w)tan\varphi^b \quad (6)$$

where τ is the shear strength of unsaturated soil, c' is the effective cohesion, σ is the total normal stress, p_a is the pore air pressure, p_w is the pore water pressure, φ' is the angle of internal friction associated with the net normal stress state variable $(\sigma - p_a)$, and φ^b is an angle indicating the rate of increase in shear strength relative to the matric suction $(p_a - p_w)$.

In this research, the residual thrust method was adopted in order to perform the slope stability analysis, incorporating matric suction and pore gas pressure. The calculation process is as follows: first the safety factor was assumed, and then the thrust was calculated from the first slide at the top of the slope to the last slide. When the thrust was equal to zero, the result of the safety factor would be the final value. Figure 2 shows the calculation diagram of the residual thrust method. The equation could be written as follows [23]:

$$\begin{aligned} P_i &= W_i sin\alpha_i - \frac{\left[c'_i l_i + \left(W_i cos\alpha_i - p^i_a l_i\right) tan\varphi'_i + l_i\left(p^i_a - p^i_w\right) tan\varphi^b\right]}{F_s} + P_{i-1}\psi_i \\ \psi_i &= \left[\cos(\alpha_{i-1} - \alpha_i) - \frac{tan\varphi'_i}{F_s}\sin(\alpha_{i-1} - \alpha_i)\right. \end{aligned} \quad (7)$$

where F_s is the safety factor of the slope, P_i is the sliding force of soil slice i, c'_i is the effective cohesive force of slice i, φ'_i is the effective internal friction angle of slice i, l_i is the width of soil slice i, W_i is the weight of soil slice i, α_i is the angle of bottom soil slice i, p^i_a and p^i_w are pore gas pressure and pore water pressure of slice i, $tan\varphi^b$ is the rate of shear strength that increases with an increase in matric suction, and ψ_i is the transfer coefficient of slice i. The model recommended by Vanapalli [24] was that $tan\varphi^b$ in the current study can be expressed as a function of effective saturation. The equation is as follows:

$$tan\varphi^b = S^* * tan\varphi' \quad (8)$$

where the effective saturation is $S^* = (S_r - S_{rw})/(1 - S_{rw})$.

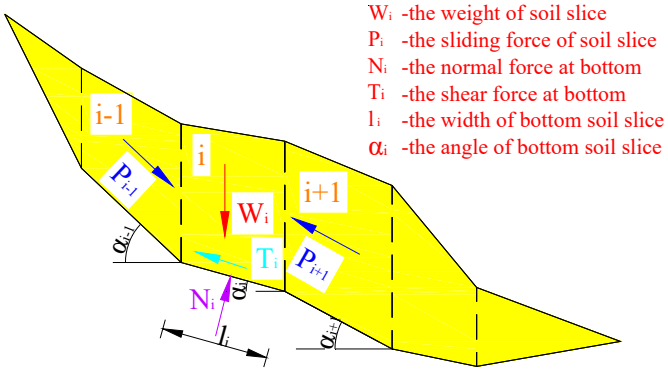

Figure 2. The calculation diagram of residual thrust method.

3.2. Slope Stability Analysis Method Considering Pore Gas Pressure

Rainfall infiltration of an unsaturated soil is a dynamic process where water and gas displace and 'squeeze' each other. When rainwater percolates downward through the soil, pore gas starts to move slowly. This can also lead to a gas pressure gradient acting on the sliding mass. Therefore, the pore gas pressure will result in the failure of the slope. In this research, the key problem was to consider the pore gas pressure gradient when evaluating slope stability.

The slope angle at the bottom of each slice is different, and the pore gas pressure cannot be considered as an internal force to be put into the residual thrust method. In

addition, pore gas pressure can be regarded as airflow that is similar to water flow when the pressure in all directions is the same value. In this study, the shape of the soil slice was assumed to be vertical, the pore gas pressure acted vertically on the boundary of each slice, and the gas pressure between two slices had the same value in opposite directions. The diagram of the residual thrust method that considers pore gas pressure is shown in Figure 3. The modified residual thrust method can be written as follows:

$$P_i = W_i sin\alpha_i - \frac{\left[c'_i l_i + \left(W_i cos\alpha_i - p^i_a l_i\right) tan\varphi'_i + l_i\left(p^i_a - p^i_w\right) tan\varphi^b\right]}{F_s} + (P_{i-1} + \Delta p_i)\psi_i$$
$$\psi_i = [\cos(\alpha_{i-1} - \alpha_i) - \frac{tan\varphi'_i}{F_s}\sin(\alpha_{i-1} - \alpha_i) \quad (9)$$

where Δp_i is the horizontal gas pressure gradient, $\Delta p_i = p^{i-1}_g - p^i_g$, and p^i_g is the pore gas pressure for slice i.

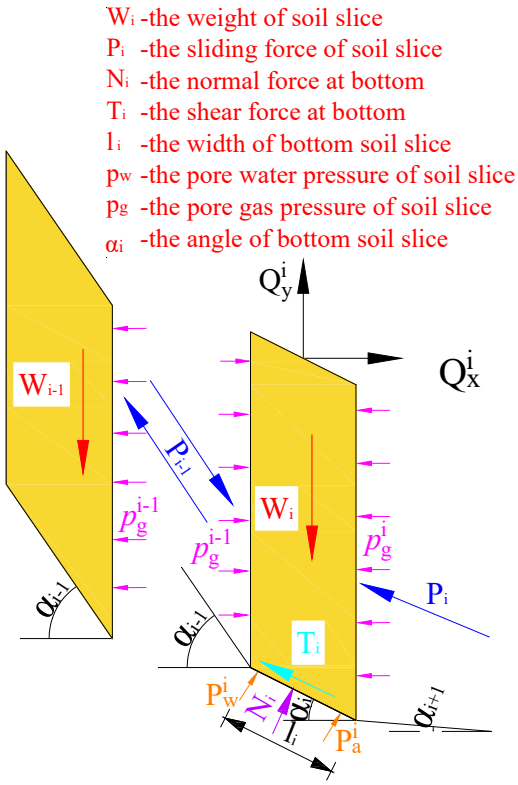

Figure 3. Diagram illustrating the calculation of the residual thrust method considering pore gas pressure.

The load variables in Equation (9) are detailed further below:

1. The weight of soil slice, W_i: the increase in the soil weight caused by infiltrated water is considered in the variable. In this calculation, the soil density is equal to the sum of the dry density of soil and the weight of water content per unit volume. 2. The shear strength parameters c_i and φ_i vary with water content, which can be tested by the shear strength test, after which the relationship between c_i, φ_i, and water moisture can also be obtained. 3. Pore gas pressure p^i_a, the gas pressure between soil slices p^i_g, and pore water pressure p^i_w can be obtained by the pore gas pressure and pore water pressure for each soil slice that is calculated by the simulation for the slope rainfall infiltration.

The variation in the weight of soil slice W_i and the shear strength parameters were closely related to the water content in the slope. The distribution of pore gas pressure, pore water pressure, and water saturation was obtained in advance to get the dynamic variation of the load on the slope. Then the load can be put into the slope analysis using the residual thrust method. In order to calculate the safety factor of slope stability accurately,

the soil should be further stratified so that the material properties of each layer are basically the same.

4. Model Studies

In order to analyze the effect of pore gas pressure on slope stability triggered by rainfall infiltration, the Tanjiahe landslide was chosen to simulate the water-air coupling process under the condition of rainfall infiltration. Then the pore gas pressure was put into the slope analysis method to analyze the impact of the pore gas pressure, caused by the movement of pore gas, on the stability of the slope.

4.1. Geometric Model Introduction

The Tanjiahe landslide was located on the right bank of the Yangtze River, and it was 56 km from the Three Gorges Dam. Located in the zone impacted by a subtropical monsoon climate, precipitation in this area was abundant with an average annual rainfall of almost 1027.5 mm, which can be the major factor that leads to landslide deformation. In this research, rainfall is characterized by uniform rainfall (5 mm/h). In addition, the main slip surface was selected as the computed section, and a two-dimensional geometric model was built with a length of 820 m and a height of 320 m (Figure 4). The pressure and matric suction of three monitoring points (H, I, J) and the pore gas pressure at the vertical section D'-D were analyzed in this research.

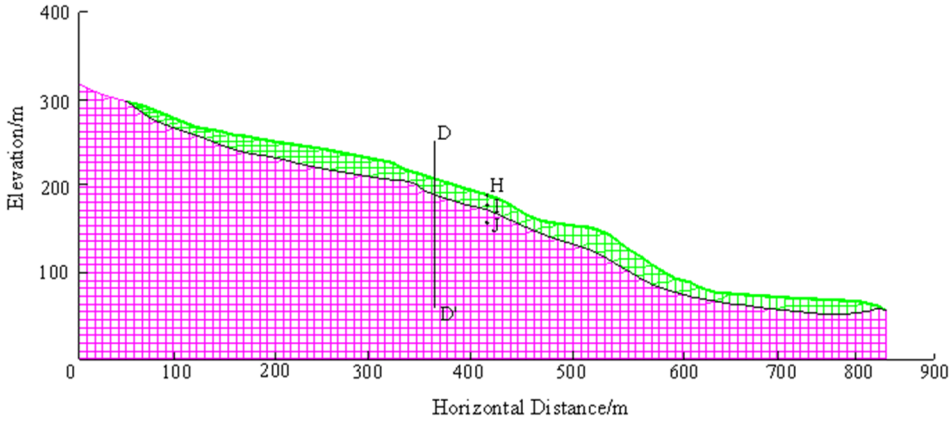

Figure 4. Finite element grid diagram of the slope cross-section.

The sliding mass was divided into vertical slices with a width of 5 m, which was equal to 5% of the slope length. As the properties of the soil were different for various water contents in the horizontal direction, the sliding mass was divided according to the different soil moisture levels.

4.2. Boundary and Initial Conditions

The surface above the reservoir water level (AB) was specified as the rainfall infiltration boundary, whereas the surface below the water level (BC) was specified as the water head boundary. Runoff was assumed to occur at the AB boundary. Runoff is assumed to occur at the AB boundary. In addition, the top surface (AB) is air-permeable, while other boundaries are impermeable to air flow.

When the rainfall intensity is less than the maximum infiltration rate of the slope body, surface runoff will not be generated; when the rainfall intensity is greater than the maximum infiltration rate of the slope body, surface runoff will be generated. As the runoff head of the slope surface is much smaller than atmospheric pressure, the runoff can be neglected in this research.

In order to reduce the influence of uncertainty on the initial condition on slope stability, the slope was considered fully saturated at the beginning. After simulating the water

infiltration for a long period, a stable state could be obtained for the entire slope. This stable state was used as the initial condition (initial saturation = 15%) for the simulation.

4.3. Material Parameters

Table 1 shows the basic values of other important parameters included in this calculation [5]. Some of the mechanical parameters for the soil were tested in the laboratory with the standard test method in China (National Standards of the People's Republic of China 1999). The parameters for shear strength are cited in the literature [25] and the values are shown in Table 2.

Table 1. Parameters for the numerical simulation.

Material parameter	*Value*
Name of parameters	silty sand
Initial intrinsic permeability (m^2)	5.8×10^{-12}
Gravitational acceleration g (m/s^2)	9.8
Residual water saturation S_{rw}	0.1
Residual gas saturation S_{rg}	0.05
Water viscosity $(kg/m{\cdot}s)$	1.0×10^{-13}
Air viscosity $(kg/m{\cdot}s)$	1.8×10^{-5}
Initial porosity	0.35
Capillary pressure : Equation (3) *with* p_0 (kPa)	1.5
Capillary pressure : Equation (3) *with m*	0.445
Initial water density (kg/m^3)	1000
Initial air density (kg/m^3)	1.25

Table 2. Shear strength parameters under different water content.

***Water Content* (%)**	***Cohesion* (*kPa*)**	***Internal Friction Angle* (o)**
	Silty Sand	**Silty Sand**
25	10.94	40.40
40	15.25	38.69
55	12.81	36.67
70	11.06	30.26
85	4.45	25.08

4.4. Results of the Simulated Rainfall Infiltration

There are two reasons why slope stability is affected by rainfall infiltration. On the one hand, rainfall infiltration is considered an external load that has a direct impact on stress and deformation, affecting the slope stability. On the other hand, the weight of the sliding areas is increased because of the infiltrated rainwater. As a result, the mechanical properties of soil are softened and the slope stability is affected indirectly. Soil bulk density, pore pressure, and shear strength are considered the main factors when evaluating slope stability. The soil bulk density for every slice is the sum of the dry density for this slice and the weight of water content per unit volume. The flow of water is also affected by the airflow in the unsaturated zone triggered by water infiltration. In return, the slope stability is also affected by this interaction of water and gas. In this study, a water-air two-phase flow analysis was carried out to evaluate the effect of water-air flow on the stability of unsaturated soil slopes. Pore gas pressure, pore water pressure, and water saturation were calculated by this simulation.

Rainfall infiltration is a coupling process in which water and air interact with each other. Especially, the effect of pore gas on rainwater infiltration is obvious. The magnitude of infiltration under unsaturated conditions mainly depends on the water phase relative permeability coefficient and the pore gas pressure gradient, while the pore water pressure gradient is affected by matric suction, pore gas pressure, as well as gravity.

4.4.1. Water-Air Coupling Effect on Rainfall Infiltration

At the onset of rainfall infiltration, the saturation of the ground surface was relatively small, so the matric suction was comparatively high. As a result, the water pressure gradient and the magnitude of infiltration were relatively high. At this time, the gas permeability coefficient for soil was relatively high and the flow of gas was good. The air could flow out of the ground surface. As the pore air pressure was close to atmospheric pressure, the effect of air on infiltration could be ignored at the ground surface in the initial stage. As the ground soil gradually reached a fully saturated state, the gas permeability coefficient decreased rapidly until the value was close to zero and could not flow anymore out of the ground surface. The pore gas increased rapidly, and the resulting pressure was the opposite direction to the water pressure because of the infiltration of water. The variation of gas pressure was much more sensitive at the location between the slope surface and the slip band. As a result, pore water pressure and the intensity of infiltration decreased. When the soil was saturated, the air pressure was equal to the water pressure and gradually stablilized, while the supporting effect of gas on the gravity gradient also tended to be stable. At this time, infiltration was mainly affected by the combined action of the matric suction and the water relative permeability coefficient in the wetting front area. This meant it was a relatively stable infiltration status.

Figure 5 shows the time series of pore gas pressure at three monitoring points (H, I, and J) in the slope. When the ground surface was saturated, it was discovered that pore gas pressure increased rapidly. This was affected by the variation of the surface ventilation condition as well as the squeezing and infiltration of water. As the degree of infiltration was relatively high in the early stage, it was too late for the pore gas generated by the extrusion to move in the soil. Therefore, there was a limit on the maximum value for the pore gas pressure (Figure 5). When the magnitude of infiltration decreased later and pore gas moved in the soil, the pore gas pressure dropped slowly and then tended to be stable. At this time, the magnitude of infiltration tended to be stable.

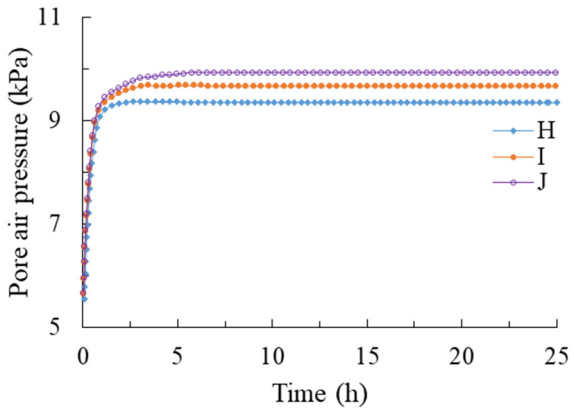

Figure 5. Time series of pore gas pressure at three monitoring points.

Figure 6 presents the development of the pore water pressure at three monitoring points (H, I, J). The evolution of pore water pressure was related to the time series from its initial negative value at the early stage of the rainfall. It was also shown that with the decrease in the distance from the slope surface, the response of pore water pressure became faster. With the infiltration of the arrival rainwater, pore water pressure increased sharply

and then finally converged to zero. The variation of the water pressure was mainly affected by the pore air pressure in the unsaturated zone.

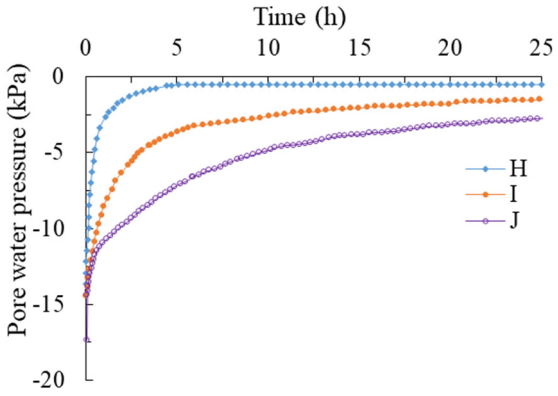

Figure 6. Time series of pore water pressure at three monitoring points.

The evolution of pore air pressure, pore water pressure, and matric suction calculated by this model at three monitoring points H, I, and J are plotted in Figure 7a–c. Matric suction decreased over time as a result of infiltrating water, but it did not converge to zero. This was because the compressed air could not escape freely through the soil surface. It was also noted that this response was different according to the distance from the slope surface. The shorter this distance, the faster the reduction of matric suction. Traditional seepage models assume that the air pressure is atmospheric. However, when air pressure and water pressure are considered, matric suction mainly comprises air pressure as well as water pressure, and it is computed as the difference between these two pressures $(p_a - p_w)$.

The gas relative permeability coefficient of the sliding bed was much larger than the sliding body; pore gas decayed along the direction of the sliding bed. The variation of pore gas pressure over depth at the slope D-D′ section is shown in Figure 8.

Contour distribution pictures including pore gas pressure, pore water pressure, and water saturation of this slope at the initial status and at the time of 2 h are shown as Figures 9 and 10. The cloud picture of saturation is shown as Figure 11.

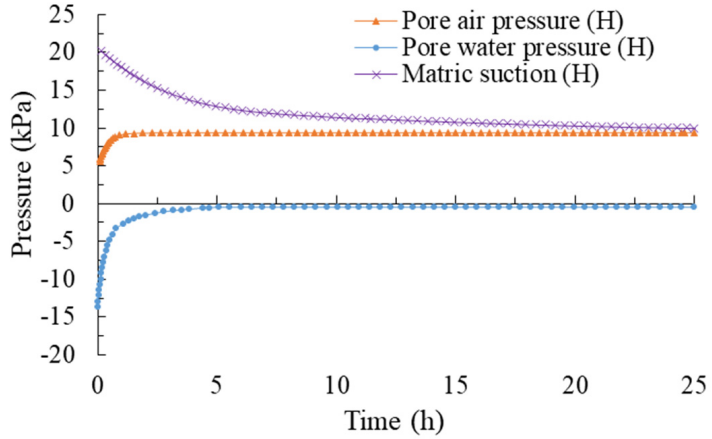

(**a**) Time series of pressure at monitoring point H

Figure 7. *Cont.*

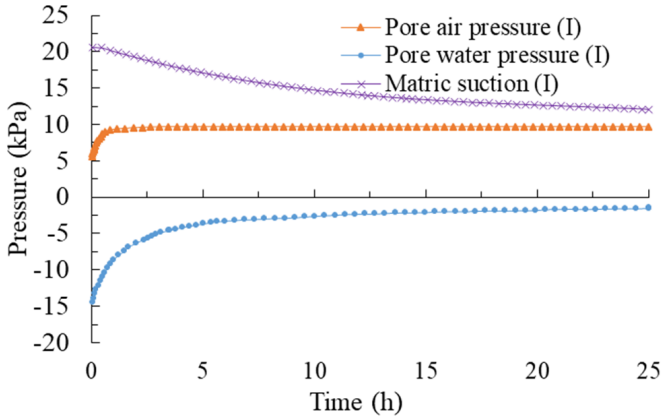

(**b**) Time series of pressure at monitoring point I

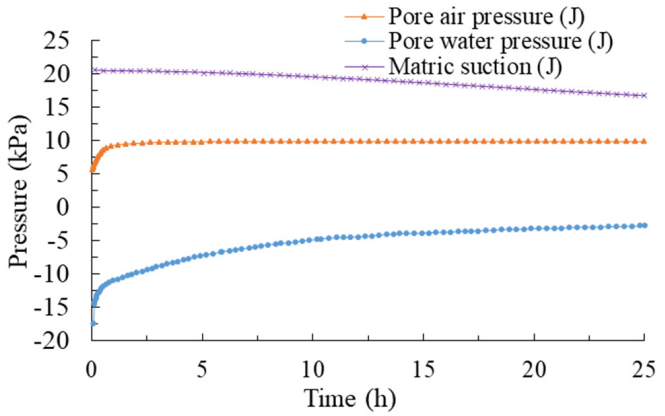

(**c**) Time series of pressure at monitoring point J

Figure 7. Time series of pressures at three monitoring points (H, I, J).

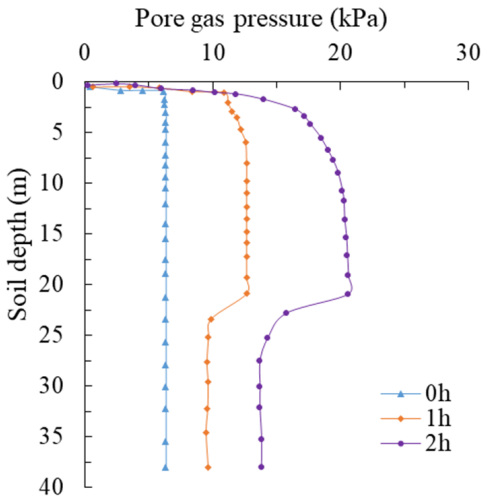

Figure 8. Pore gas pressure distribution in depth over time.

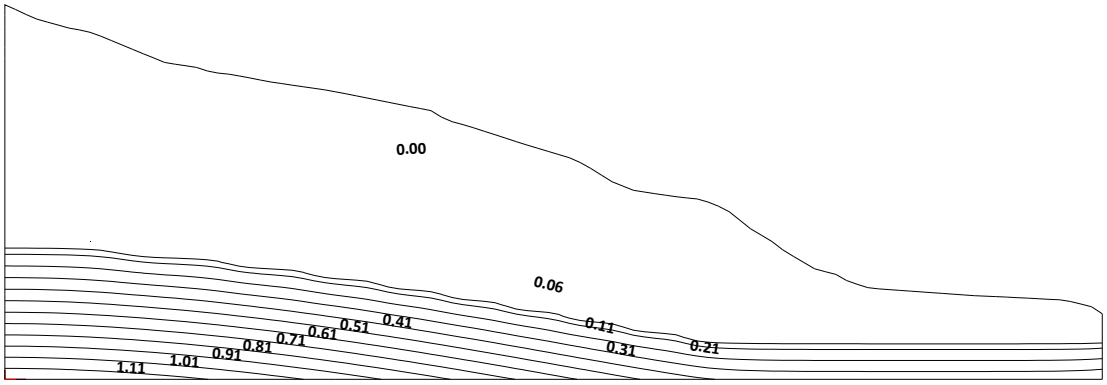

(**a**)Pore gas pressure (MPa)

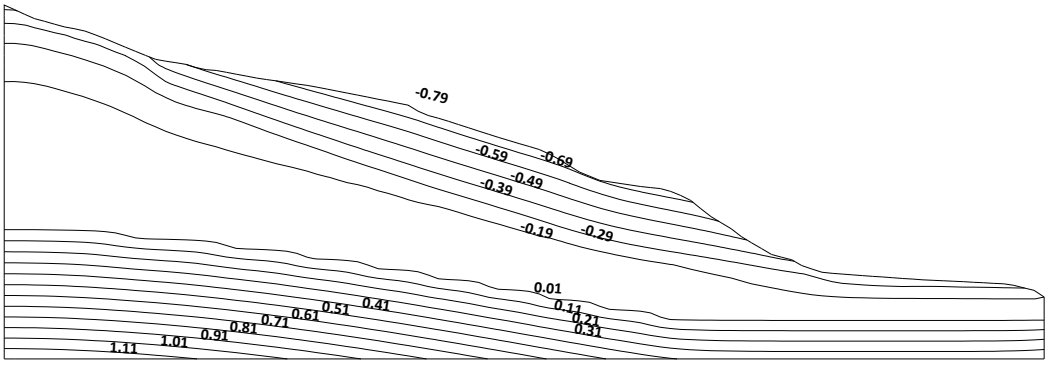

(**b**)Pore water pressure (MPa)

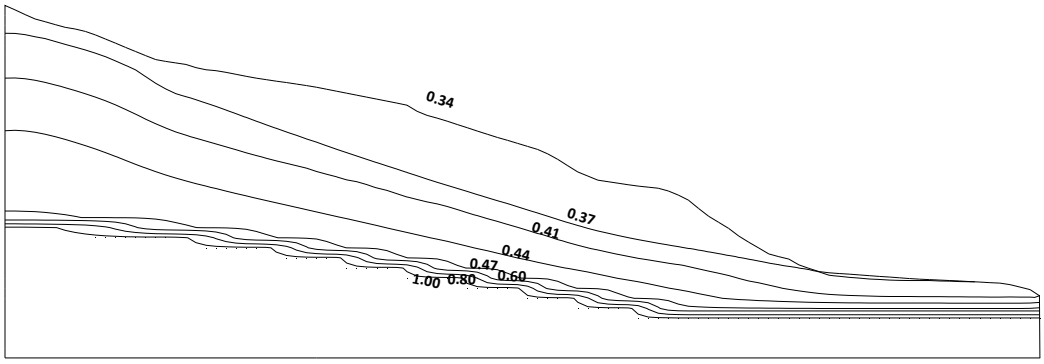

(**c**)Water saturation

Figure 9. Contour distribution pictures of three parameters at initial status.

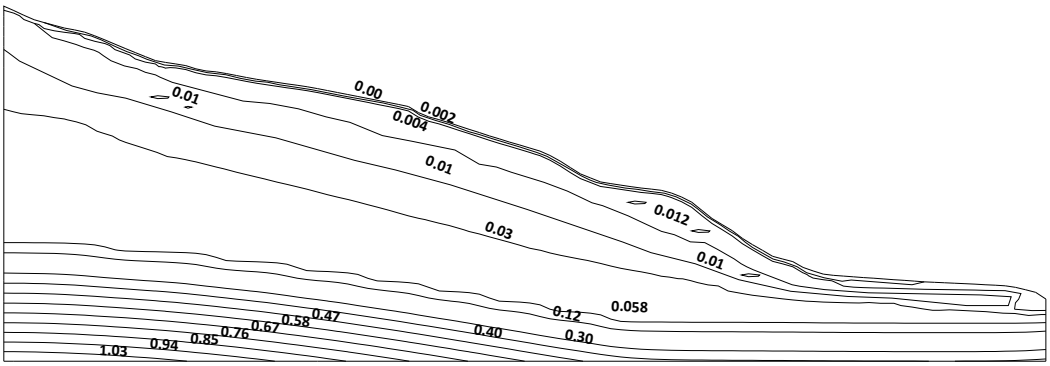

(**a**) Pore gas pressure (MPa)

Figure 10. *Cont.*

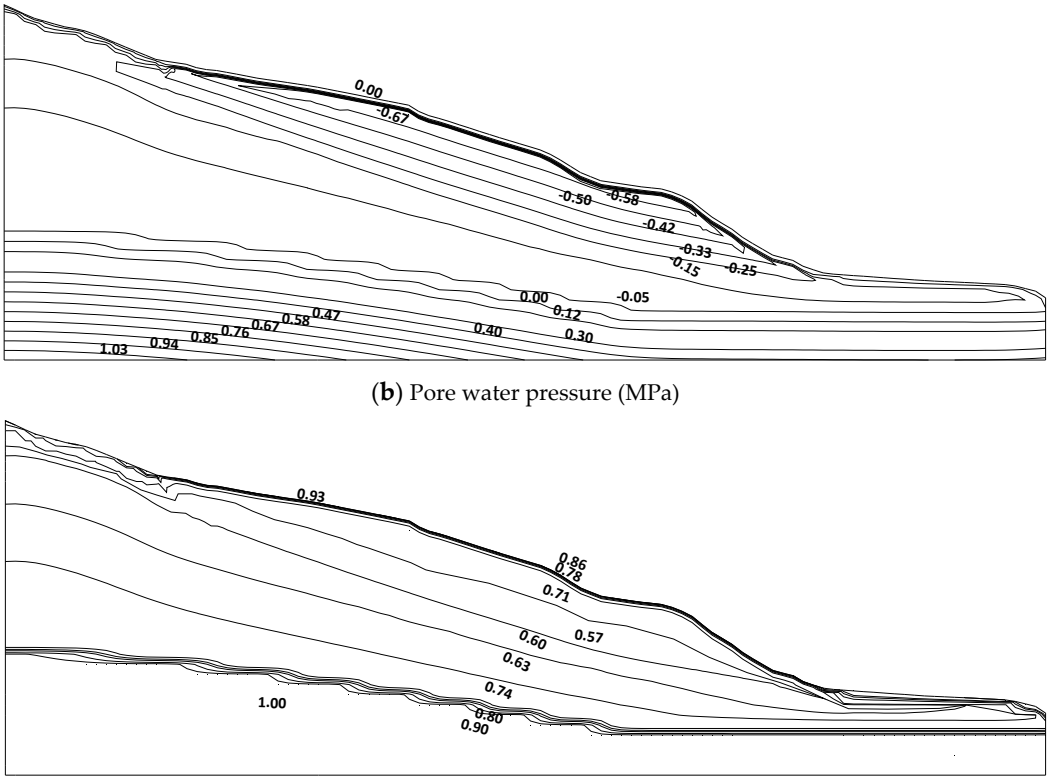

(**b**) Pore water pressure (MPa)

(**c**) Water saturation

Figure 10. Contour distribution pictures of three parameters at the rainfall time of 2 h.

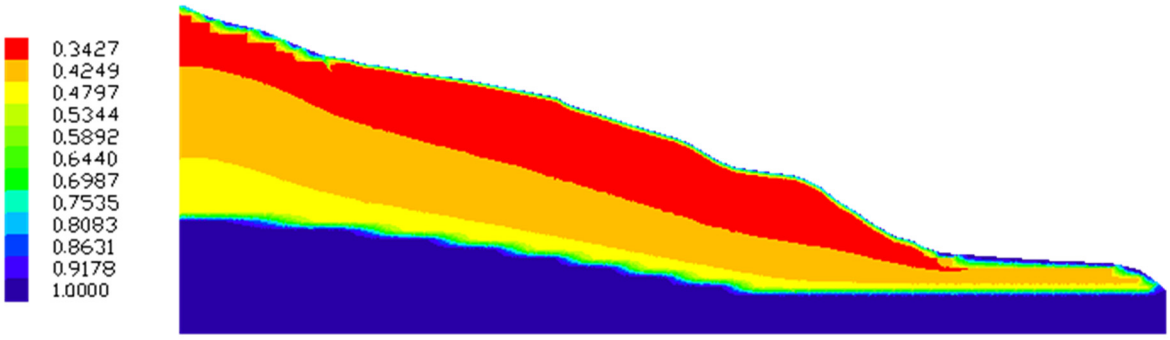

Figure 11. Cloud picture of saturation distribution at the rainfall time of 2 h.

4.4.2. The Effect of Initial Saturation on Rainfall Infiltration

Figure 12a,b depict vertical profiles of saturation at section D-D′ for an initial saturation of 60% and 15%, respectively. At the onset of the rainfall, it was also difficult for pore air to flow out through the slope surface because of the saturated ground surface. Therefore, the pores were occupied by pore air, and a somewhat unsaturated state was continued above the wetting front even during torrential rain. Figure 12a,b demonstrate that the degree of saturation was closely related to the initial saturation. As the gas relative permeability coefficient decreased with the increased initial saturation (Figure 1), pore gas pressure increased gradually. Moreover, the increase of matric suction was closely correlated with increased pore gas pressure, while the water content of the soil surface with 60% initial saturation was much less than that with 15% initial saturation. In addition, water infiltration was greatly affected by pore gas pressure when the saturation of the soil surface was relatively low. When the initial saturation reached the saturation point, water infiltrated the

pore channel because the pore gas was relatively low. This also demonstrated that water infiltration was weakly affected by pore gas pressure.

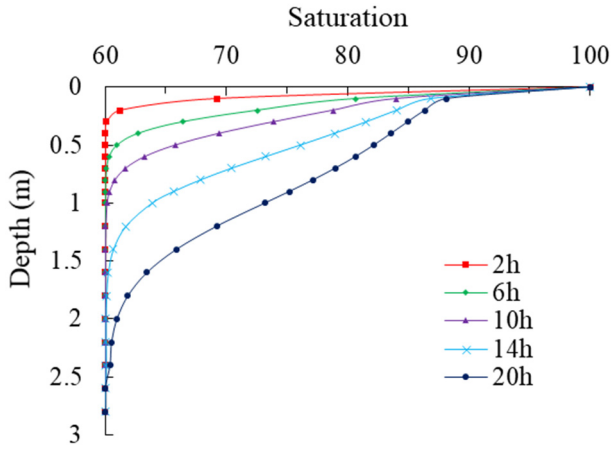

(**a**) Initial saturation = 60%

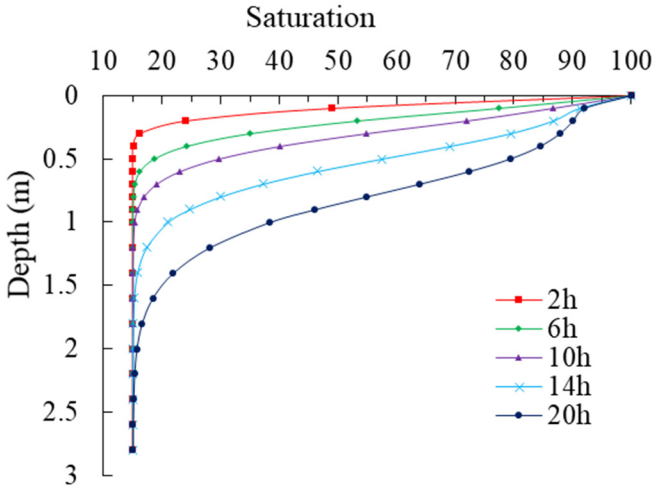

(**b**) Initial saturation = 15%

Figure 12. Saturation distribution in depth over time at various initial saturation degrees.

As the initial saturation increased, the content of pore gas decreased, and the channels for water infiltration and water relative permeability coefficient increased (Figure 1). Matric suction increases with a decreasing initial saturation, resulting in an increase in water inflow. When the water relative permeability coefficient decreases, the water outflow decreases. As a result, a steep wetting front appears because of the difference between inflow and outflow intensity.

4.4.3. The Effect of Initial Saturation on Rainfall Infiltration

This study researched the infiltration intensity for a stable period in order to compare the relationship between infiltration intensity and initial saturation. During this period, pore gas pressure tended to be stable, and the support effect of gas on the gravity gradient also stopped. The magnitude of infiltration was affected by matric suction, water, and gas permeability characteristics, and the support for gravity gradient could be ignored. In this research, the rainfall infiltration magnitude was described by the relative infiltration magnitude, which was a dimensionless variable. It was defined as the ratio of the rainwater infiltration rate to the saturated permeability coefficient of soil.

At the onset of rainfall infiltration, the magnitude of infiltration was mainly affected by the matric suction on the soil surface; the pore water pressure gradient rose because of the higher matric suction. Therefore, the magnitude of infiltration was relatively large at this time because the saturation of the soil surface was low (Figure 13). When infiltration tended to be stable, infiltration was mainly affected by the matric suction and the water relative permeability coefficient at the location of the wetting front. As shown in Figure 14, the stable magnitude of infiltration first declined, then grew with the increase of saturation. The maximum value of stable magnitude for infiltration occurred at the residual saturation (effective saturation = 0) or fully saturated status (effective saturation = 1). The minimum value of stable magnitude for infiltration occurred at the unsaturated status. Initially, as initial saturation was lower, the infiltrated water was driven by matric suction. When the initial saturation increased, although matric suction continued to decrease, the water relative permeability coefficient increased rapidly, and as a result, rainfall infiltration occurred at a minimum value. With the increase of initial saturation, the effect of matric suction on infiltration continued to decrease, and the water relative coefficient of permeability tended to be one (Figure 1), so the water was infiltrated by the pore channels. During this period, the infiltration magnitude was mainly affected by the water relative permeability coefficient. Therefore, the magnitude of infiltration increased with the increase of initial saturation during this period. The maximum value of stable magnitude infiltration for silty sand occurred at the residual saturation, while the minimum value for it occurred at a saturation between 80% and 90%.

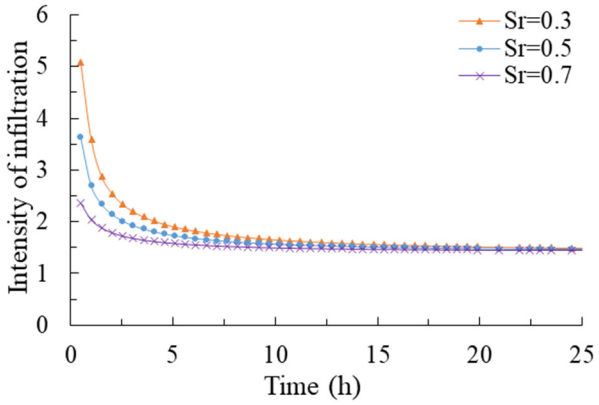

Figure 13. Time series for the intensity of infiltration at different saturation degrees.

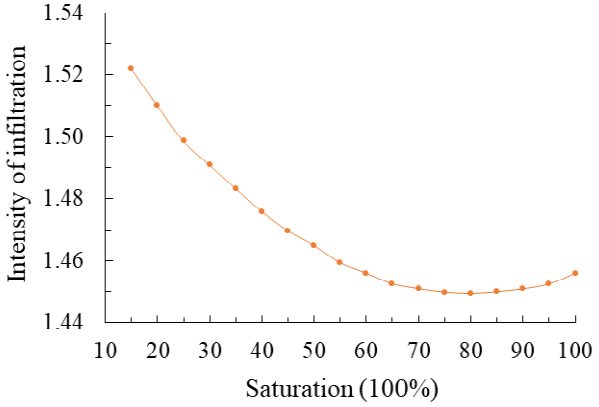

Figure 14. Diagram of infiltration intensity with saturation degree.

4.4.4. The Effect of Water-Gas Coupling Effect on Slope Stability

In order to research the effect of pore gas pressure on slope stability, the safety factor was calculated for two cases. The variation of soil bulk density and shear strength parame-

ters caused by rainfall infiltration instead of pore gas pressure was considered for the first case. Pore gas pressure was added in the second case to analyze the slope stability.

Figure 15 depicts the safety factor in two cases when considering the water-gas coupling effect and not. At the onset of rainfall infiltration, the ground surface was unsaturated, and the gas relative permeability coefficient was relatively high, so that enclosed pressure could not be formed on the slope and the variation for the safety factor was not obvious. With continuous rainwater seepage, the safety factor declined in the two cases because of the increase in sliding weight and pore gas pressure. When the soil surface was saturated, pore gas pressure increased rapidly because of the infiltration displacement and extrusion of rainwater. While the gas relative permeability coefficient was relatively small, air could not flow out of the ground surface. As a result, the water pressure in the saturated surface zone could be transferred by pore gas pressure to the toe of the slope, and a pore gas pressure gradient was created along the direction of the slope toe (Figure 10). This was the negative influence of the gas force on the slope stability. When calculating the safety factor considering the water-gas coupling effect, the slope failed. This could also be a risk for slope stability when calculating the safety factor by using the traditional residual thrust method. Therefore, the method proposed by this study was much safer when evaluating slope stability.

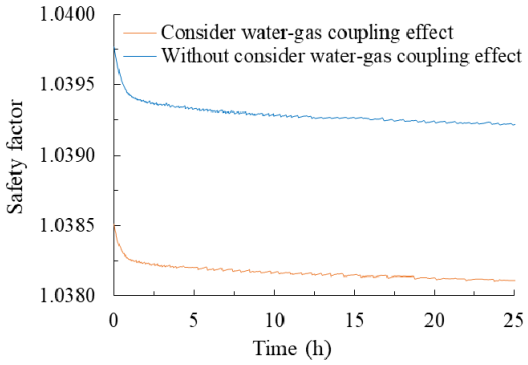

Figure 15. Evolution of safety factor over time.

The results analyzed above for the two cases are demonstrated by the residual thrust distribution diagram in Figure 16. The two areas on this slope include the promote slide zone and the prevent slide zone. The horizontal projection of the promote slide zone was about 460 m, and the prevent slide zone was about 360 m. When calculating residual thrust, considering the pore gas pressure, the residual thrust between soil stripes increased. In addition, the rise in the promote slide zone was much larger than the prevent slide zone, which can lead to an increase in sliding force, and the slope stability was reduced.

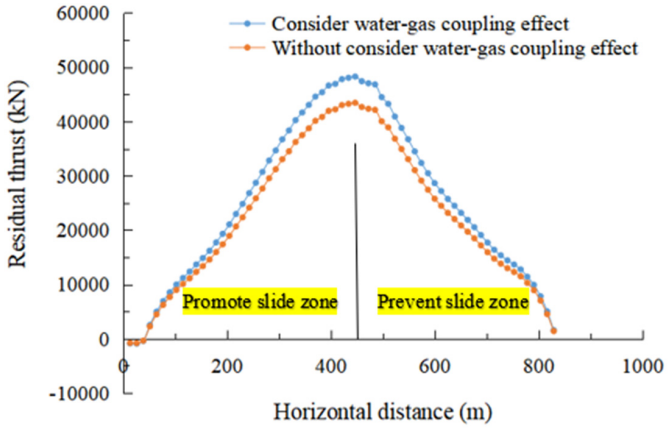

Figure 16. Diagram of the distribution of residual thrust.

4.4.5. The Effect of Initial Saturation on Slope Stability

Figure 17 shows the evolution of the safety factor for different saturation degrees when considering the water-gas coupling effect. It shows that the safety factor decreases with increasing initial saturation. When the saturation was more than 85%, the degree of decline of the safety factor became slower than when the saturation degree was less than 85%. This is the result of an increasing magnitude of infiltration with a saturation degree of more than 85%.

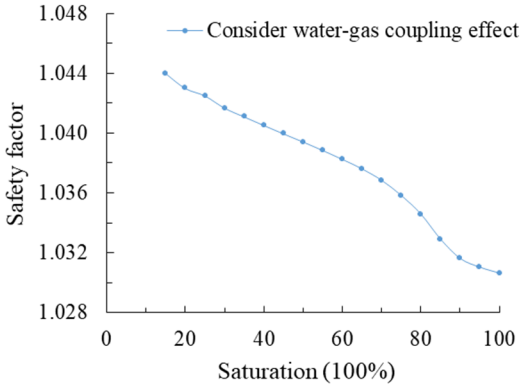

Figure 17. Evolution of safety factor with saturation degree.

Figure 18 shows the diagram for the distribution of residual thrust for various saturations. The residual thrust under the initial saturation of 70% was much more than that at an initial saturation of 30%. This also explains why the safety factor decreases with increasing initial saturation.

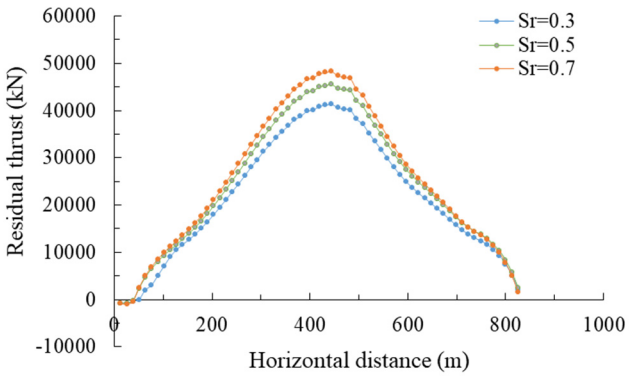

Figure 18. Diagram for distribution of residual thrust for different saturation degrees.

5. Conclusions

In this study, a water-air two-phase flow analysis was conducted in order to study the effect of pore gas pressure caused by rainfall infiltration on the stability of unsaturated soil slopes. During this process, the variation of the load as a result of the pore gas pressure was obtained. Together with the unsaturated soil shear strength theory and the residual thrust method, pore gas pressure was incorporated into the slope stability analysis method. In order to compare the infiltration behavior with respect to initial saturation, we investigated the movement of pore gas pressure and pore water pressure for silty sand. The following conclusions could be drawn from the analysis:

(1) When the ground surface of the soil approached the saturated condition, the pore gas was squeezed by infiltrated water, and the support for the gas opposite to the gravity gradient occurred. Therefore, the magnitude of infiltration decreased and tended to be stable because of the support of gas, and the stable infiltration magnitude was mainly affected by matric suction and the water relative permeability coefficient. When there was

low saturation, the stable magnitude of infiltration was mainly affected by matric suction and decreased as the saturation increased. When the saturation approached 100%, the magnitude of infiltration was mainly affected by the water relative permeability coefficient, and it increased with the increase in the degree of saturation.

(2) The maximum value of stable infiltration magnitude occurred at the residual saturation degree (saturation = 0%) or at saturation (saturation = 100%). This value was affected by the soil-water characteristic curve as well as the water and gas relative permeability coefficients. In this research, the maximum value of the stable magnitude of infiltration for silty sand occurred at the degree of residual saturation, while the minimum value for it occurred at saturation levels between 80% and 90%. When the saturation was more than 85%, the degree of declination for the safety factor became slower compared with a saturation degree of less than 85%. This was because the magnitude of infiltration increased when the saturation degree was more than 85%.

(3) During the process of infiltration, it was difficult for the ground surface soil to reach full saturation. The greater the initial saturation was, the greater the pore gas pressure and the stronger the influence of gas on the soil saturation. The saturation by the soil surface was much smaller. In addition, affected by the water relative permeability coefficient, water was infiltrated by the matric suction gradient at the higher gas content and water was infiltrated by the pore channel at the lower gas content.

(4) As the coefficient of viscosity for air is much smaller than for water, the flow of air is much better than the flow of water. As a result, pore water pressure in the saturated zone can be transferred to the toe of the slope by pore gas pressure. This could also result in a pore gas pressure gradient oriented towards the slope's toe, increasing the thrust for the slipping mass. This mechanism of force transfer has a negative impact on the safety factor.

(5) This research adopted the results of the calculation of stress and seepage using the finite element method. The pore gas pressure in the unsaturated zone and the pore water pressure in the saturated zone were as a result of the gradient. In addition, the impact of the saturation degree on the slope stability was realized by modifying the shear strength parameters, cohesion, and internal friction angle. When analyzing slope stability, this method is much safer than other traditional methods.

Author Contributions: Conceptualization, W.T. and H.P.; methodology, W.T.; software, S.X.; validation, W.T., H.P. and B.M.; formal analysis, Z.C.; investigation, W.T.; resources, Z.C.; data curation, H.P.; writing—original draft preparation, W.T.; writing—review and editing, H.P.; visualization, S.X.; supervision, H.P.; project administration, H.P.; funding acquisition, H.P. All authors have read and agreed to the published version of the manuscript.

Funding: The work was supported by the Geotechnical Laboratory at Ghent University. The first author would like to acknowledge the financial support received from the China Scholarship Council (No.201908420298).

Institutional Review Board Statement: Not applicable.

Informed Consent Statement: Not applicable.

Data Availability Statement: Not applicable.

Acknowledgments: The work was supported by the Geotechnical Laboratory at Ghent University and some colleagues in China Three Gorges University.

Conflicts of Interest: The authors declare no conflict of interest.

References

1. Bear, J.; Bachmat, Y. Deletion of nondominant effects in modeling transport in porous media. *Transp. Porous Media* **1992**, *7*, 15–38. [CrossRef]
2. Chen, H.; Lee, C.F.; Law, K.T. Causative mechanisms of rainfall-induced fill slope failures. *J. Geotech. Geoenviron. Eng.* **2004**, *130*, 593–602. [CrossRef]
3. Chen, Z.-Y.; Shao, C.-M. Evaluation of minimum factor of safety in slope stability analysis. *Can. Geotech. J.* **1988**, *25*, 735–748. [CrossRef]

4. Cho, S.E. Stability analysis of unsaturated soil slopes considering water-air flow caused by rainfall infiltration. *Eng. Geol.* **2016**, *211*, 184–197. [CrossRef]
5. Corey, A.T. The interrelation between gas and oil relative permeabilities. *Prod. Mon.* **1954**, *19*, 38–41.
6. Fang, N.; Ji, C.; Crusoe, G.E. Stability analysis of the sliding process of the west slope in Buzhaoba Open-Pit Mine. *Int. J. Min. Sci. Technol.* **2016**, *26*, 869–875. [CrossRef]
7. Fredlund, D.G.; Morgenstern, N.R.; Widger, R.A. The shear strength of unsaturated soils. *Can. Geotech. J.* **1978**, *15*, 313–321. [CrossRef]
8. Gao, Y.S.; Liu, C.; Tian, W.; Zhao, Y. Experimental Study on the Relationship Between Saturation and Shear Strength of Silty Clay. *Pearl River Chin.* **2018**, *39*, 1–4.
9. Hu, R.; Chen, Y.; Zhou, C. Modeling of coupled deformation, water flow and gas transport in soil slopes subjected to rain infiltration. *Sci. China Technol. Sci.* **2011**, *54*, 2561–2575. [CrossRef]
10. Igwe, O.; Mode, W.; Nnebedum, O.; Okonkwo, I.; Oha, I. The analysis of rainfall-induced slope failures at Iva Valley area of Enugu State, Nigeria. *Environ. Earth Sci.* **2013**, *71*, 2465–2480. [CrossRef]
11. Liu, G.; Tong, F.-G.; Zhao, Y.-T.; Tian, B. A force transfer mechanism for triggering landslides during rainfall infiltration. *J. Mt. Sci.* **2018**, *15*, 2480–2491. [CrossRef]
12. Liu, S.; Shao, L.; Li, H. Slope stability analysis using the limit equilibrium method and two finite element methods. *Comput. Geotech.* **2014**, *63*, 291–298. [CrossRef]
13. Michalowski, R.L. Limit analysis and stability charts for 3D slope failures. *J. Geotech. Geoenviron. Eng.* **2010**, *136*, 583–593. [CrossRef]
14. Mualem, Y. A new model for predicting the hydraulic conductivity of unsaturated porous media. *Water Resour. Res.* **1976**, *12*, 513–522. [CrossRef]
15. Song, Z.F.; Xu, X.M. Brief introduction of residual thrust method and its improvement. *Appl. Mech. Mater.* **2012**, *166–169*, 3358–3363. [CrossRef]
16. Su, Z.; Shao, L. A three-dimensional slope stability analysis method based on finite element method stress analysis. *Eng. Geol.* **2020**, *280*, 105910. [CrossRef]
17. Sun, D.-M.; Zang, Y.-G.; Semprich, S. Effects of airflow induced by rainfall infiltration on unsaturated soil slope stability. *Transp. Porous Media* **2015**, *107*, 821–841. [CrossRef]
18. Tong, F. *Numerical Modeling of Coupled Thermo-Hydro-Mechanical Processes in Geological Porous Media*; KTH: Stockholm, Sweden, 2010.
19. Tong, F.; Jing, L.; Zimmerman, R.W. A fully coupled thermo-hydro-mechanical model for simulating multiphase flow, deformation and heat transfer in buffer material and rock masses. *Int. J. Rock Mech. Min. Sci.* **2010**, *47*, 205–217. [CrossRef]
20. Van Genuchten, M.T. A closed-form equation for predicting the hydraulic conductivity of unsaturated soils. *Soil Sci. Soc. Am. J.* **1980**, *44*, 892–898. [CrossRef]
21. Vanapalli, S.K.; Sillers, W.S.; Fredlund, M.D. The meaning and relevance of residual state to unsaturated soils. In *51st Canadian Geotechnical Conference*; The Canadian Geotechnical Society: Edmonton, AB, Canada, 1998.
22. Wang, B.; Vardon, P.; Hicks, M. Rainfall-induced slope collapse with coupled material point method. *Eng. Geol.* **2018**, *239*, 1–12. [CrossRef]
23. Wu, L.Z.; Huang, R.Q.; Xu, Q.; Zhang, L.M.; Li, H.L. Analysis of physical testing of rainfall-induced soil slope failures. *Environ. Earth Sci.* **2015**, *73*, 8519–8531. [CrossRef]
24. Wu, L.Z.; Selvadurai, A.P.S. Rainfall infiltration-induced groundwater table rise in an unsaturated porous medium. *Environ. Earth Sci.* **2016**, *75*, 135. [CrossRef]
25. Zhang, X.-Y.; Zhu, Y.-M.; Fang, C.-H. The role fore air flow in soil slope stability analysis. *J. Hydrodyn.* **2009**, *21*, 640–646. [CrossRef]